Supplementary data for article:

Todorovic, T.; Grubišic, S.; Pregelj, M.; Jagodič, M.; Misirlic-Denčic, S.; Dulovic, M.; Markovic, I.; Klisuric, O.; Maleševic, A.; Mitic, D.; et al. Structural, Magnetic, DFT, and Biological Studies of Mononuclear and Dinuclear CuII Complexes with Bidentate N-Heteroaromatic Schiff Base Ligands. *European Journal of Inorganic Chemistry* **2015**, *2015* (23), 3921–3931. https://doi.org/10.1002/ejic.201500349

Eur. J. Inorg. Chem. **2015** · ISSN 1099–0682

SUPPORTING INFORMATION

DOI: 10.1002/ejic.201500349
Title: Structural, Magnetic, DFT, and Biological Studies of Mononuclear and Dinuclear Cu^{II} Complexes with Bidentate N-Heteroaromatic Schiff Base Ligands
Author(s): Tamara Todorović, Sonja Grubišić, Matej Pregelj, Marko Jagodič, Sonja Misirlić-Denčić, Marija Dulović, Ivanka Marković, Olivera Klisurić, Aleksandar Malešević, Dragana Mitić, Katarina Anđelković, Nenad Filipović*

Results and Discussion

Synthesis of the complexes 1 and 2 and their interconversion

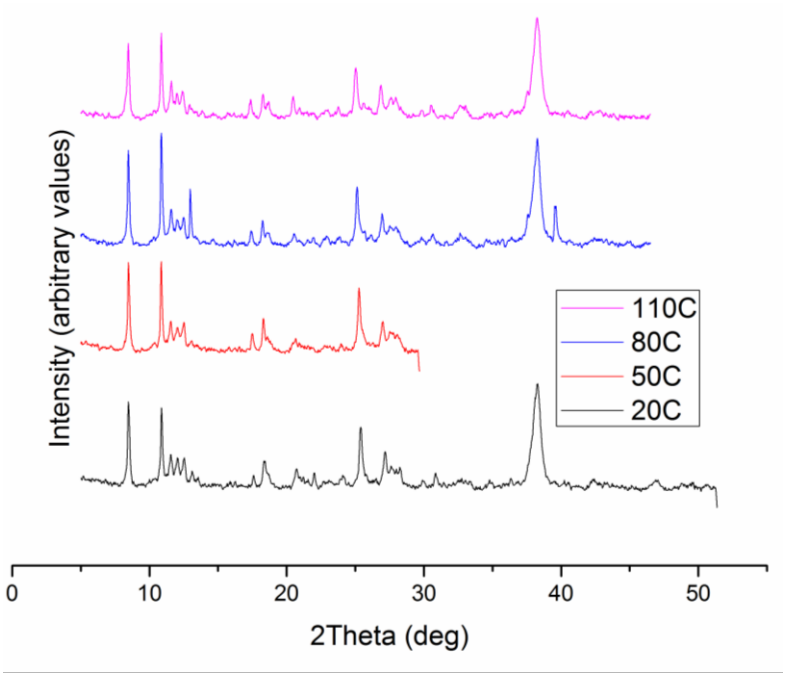

Figure S1. Diffractograms for complex **1** obtained on heating.

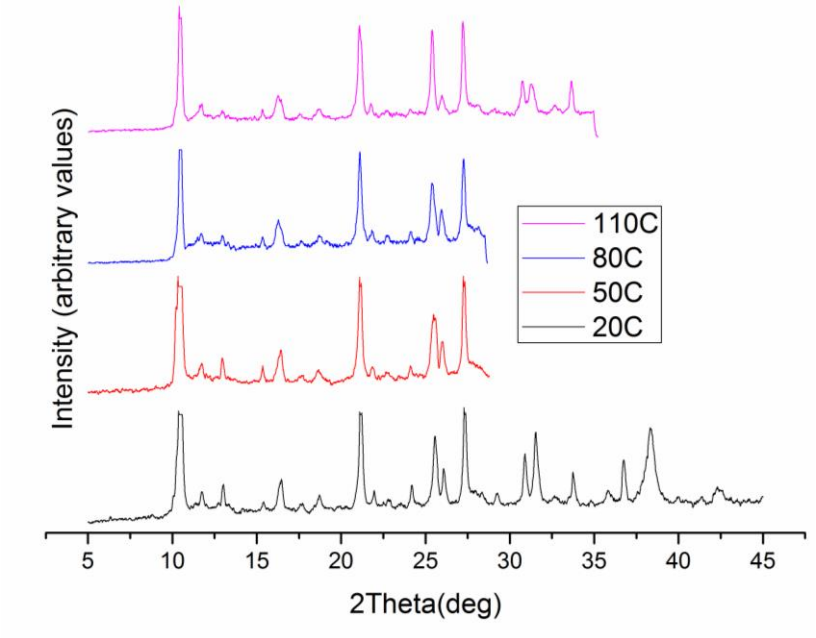

Figure S2. Diffractograms for complex **2** obtained on heating.

Analysis of Crystal Structures

Table S1. Crystal data and structure refinement for copper(II) complexes **1** and **2**

Compound	$[CuCl_2(aphaOMe)]$ (**1**)	$[Cu_2Cl_4(aphaOMe)_2]$ (**2**)
Empirical formula	$C_{10}H_{13}Cl_2CuN_3O_2$	$C_{20}H_{26}Cl_4Cu_2N_6O_4$
Formula weight	341.67	683.35
Temperature (K)	293(2)	293(2)
Wavelength (Å)	0.71073	0.71073
Crystal system	Triclinic	Monoclinic
Space group	*P* -1	*P* $2_1/n$
Unit cell dimensions	*a* = 7.4591(7) Å	*a* = 9.0304(3) Å
	b = 9.0156(5) Å	*b* = 13.8032(4) Å
	c = 11.3223(10) Å	*c* = 10.9337(4) Å
	α = 101.220(6)°	α = 90°
	β = 105.312(8)°	β = 100.752(3)°
	γ = 109.259(7)°	γ = 90°
Volume ($Å^3$)	659.27(9)	1338.94(8)
Z	2	2
D_{calc} ($Mg\ m^{-3}$)	1.721	1.695
Absorption coefficient (mm^{-1})	2.058	2.026
F(000)	346	692
Theta range for data collection (°)	3.02 to 25.00	2.95 to 25.00
Reflections collected	3936	5372
Independent reflections	2318 [R(int) = 0.0194]	2351 [R(int) = 0.0266]
Completeness to theta = 25.00°	99.9 %	99.8 %
Absorption correction	Semi-empirical from equivalents	Semi-empirical from equivalents
Max. and min. transmission	1.00000 and 0.98190	1.00000 and 0.95290
Refinement method	Full-matrix least-squares on F^2	Full-matrix least-squares on F^2
Data / restraints / parameters	2318 / 0 / 215	2351 / 0 / 193
Goodness-of-fit on F^2	1.082	1.069
Final R indices [I >2sigma(I)]	R1 = 0.0351, wR2 = 0.0745	R1 = 0.0372, wR2 = 0.0805
R indices (all data)	R1 = 0.0430, wR2 = 0.0783	R1 = 0.0471, wR2 = 0.0851
Largest diff. peak and hole ($e\ Å^{-3}$)	0.391 and -0.260	0.623 and -0.415

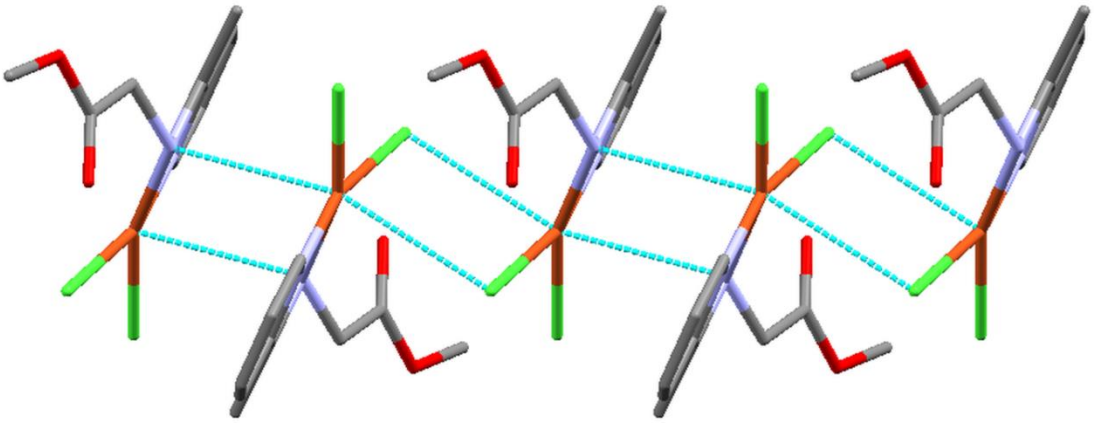

Figure S3. Infinite one-dimensional chains parallel to the *a*-axis in the crystal structure of complex **1**. View direction is close to *c*-axis.

Table S2. C–H…O interaction parameters for **2**

C–H···O	r(C–H) (Å)	r(H···O) (Å)	r(C···O) (Å)	Angle C–H···O (°)	Symmetry
C(4)–H(4)···O(1)	0.87	2.70	3.240(5)	122	$1 - x, 1 - y, 1 - z$
C(5)–H(5)···O(1)	0.95	2.67	3.267(5)	121	$1 - x, 1 - y, 1 - z$

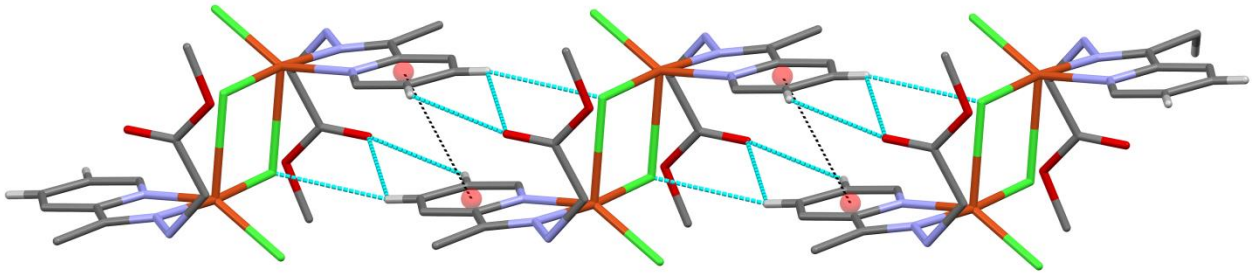

Figure S4. One-dimensional supramolecular chain along [100] direction formed by binuclear units of complex **2**. Black dashed lines indicate π-π stacking interactions of pyridine fragments while blue dashed lines indicate C–H···O interactions.

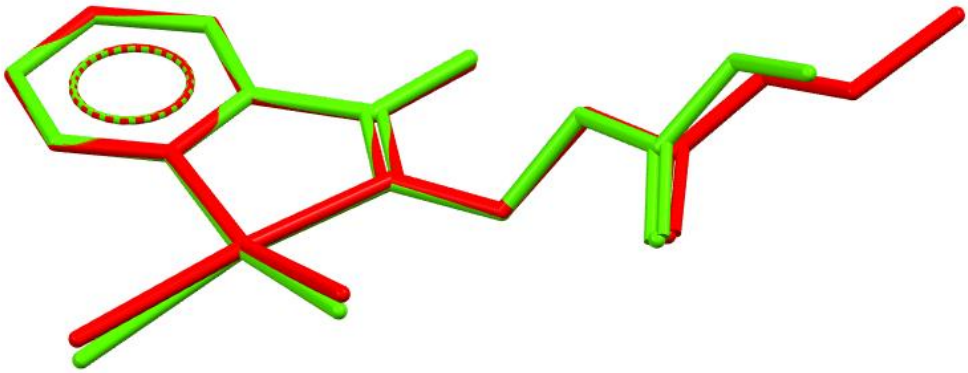

Figure S5. The result of a least-squares fit of the aromatic frames of complexes **1** (green) and **4** (red). Hydrogen atoms have been omitted for clarity. Main directions of the side chains are separated by cca. 5°.

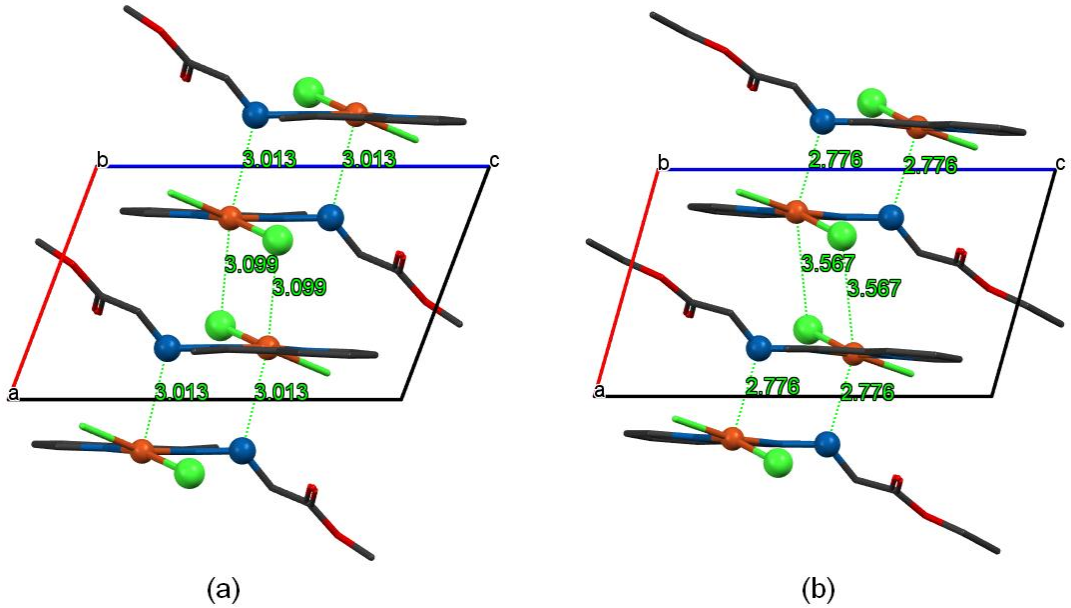

Figure S6. Packing of molecules in the crystal structures of complexes **1** (a) and **4** (b). Hydrogen atoms are omitted for clarity. Color code: gray – C, blue – N, red – O, green – Cl, dark orange – Cu.

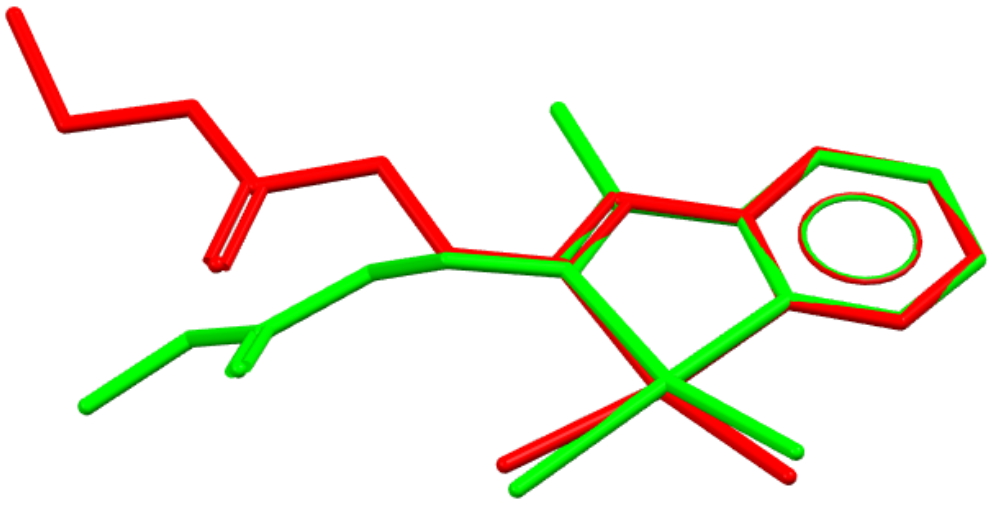

Figure S7. The result of a least-squares fit of the aromatic frames of complexes **1** (green) and **3** (red). Hydrogen atoms have been omitted for clarity. Main directions of the side chains are separated by cca. 54°.

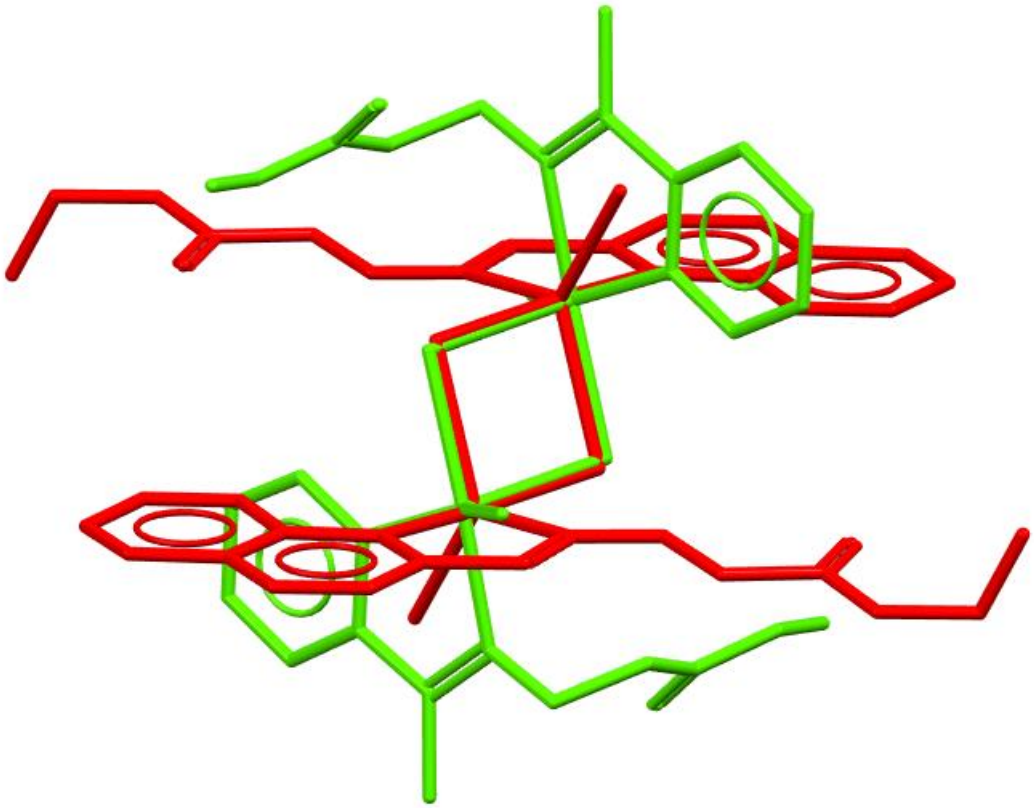

Figure S8. The result of a least-squares fit of the Cu–(μ-Cl)$_2$–Cu skeleton of complexes **2** (green) and **5** (red). Hydrogen atoms have been omitted for clarity.

Electronic absorption spectroscopy and molar conductivity measurements

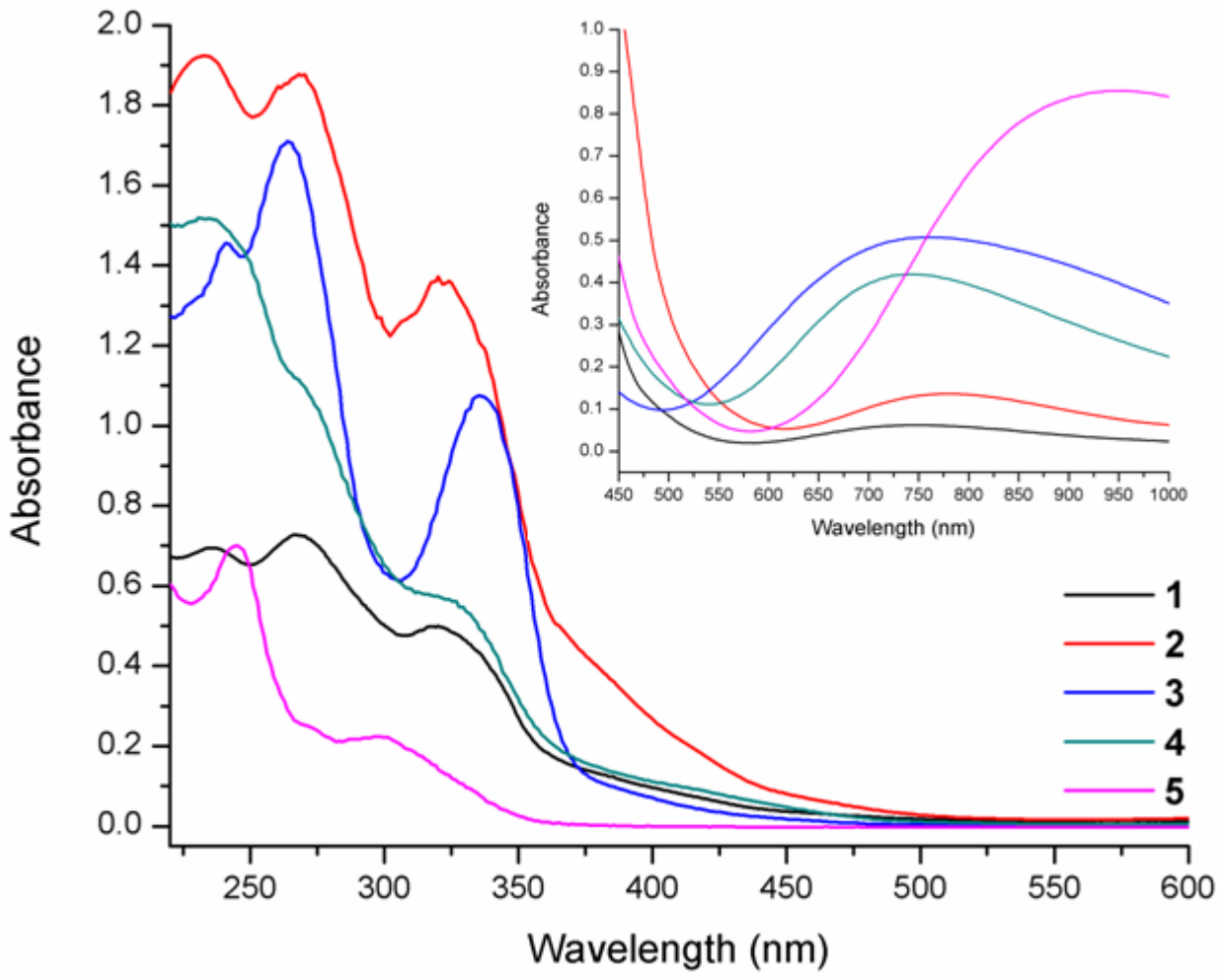

Figure S9. The electronic absorption spectra of complexes **1**–**5** in DMSO/H_2O 0.5 : 100 (*v*/*v*) at 298 K ($c_{\mathbf{1,2}}$ = 5 × 10^{-5} M; $c_{\mathbf{3,4}}$ = 1 × 10^{-4} M; $c_{\mathbf{5}}$ = 1 × 10^{-5} M). Inset: The electronic absorption spectra of complexes **1**–**5** in DMSO/H_2O 0.5 : 100 (v/v) at 298 K ($c_{\mathbf{1,2}}$ = 1 × 10^{-3} M; $c_{\mathbf{3}}$ = 5 × 10^{-3} M; $c_{\mathbf{4}}$ = 4.8 × 10^{-3} M; $c_{\mathbf{5}}$ = 4.5 × 10^{-3} M).

Table S3. Electronic spectral data for complexes **1**–**5**.

Complex	λ_{max} / nm
1	235, 269, 320, 749, 752[a]
2	233, 268, 322, 783, 786[a]
3	240, 264, 336, 751
4	234, 269sh, 328, 742
5	245, 272sh, 200, 942

[a] In diffuse reflectance.

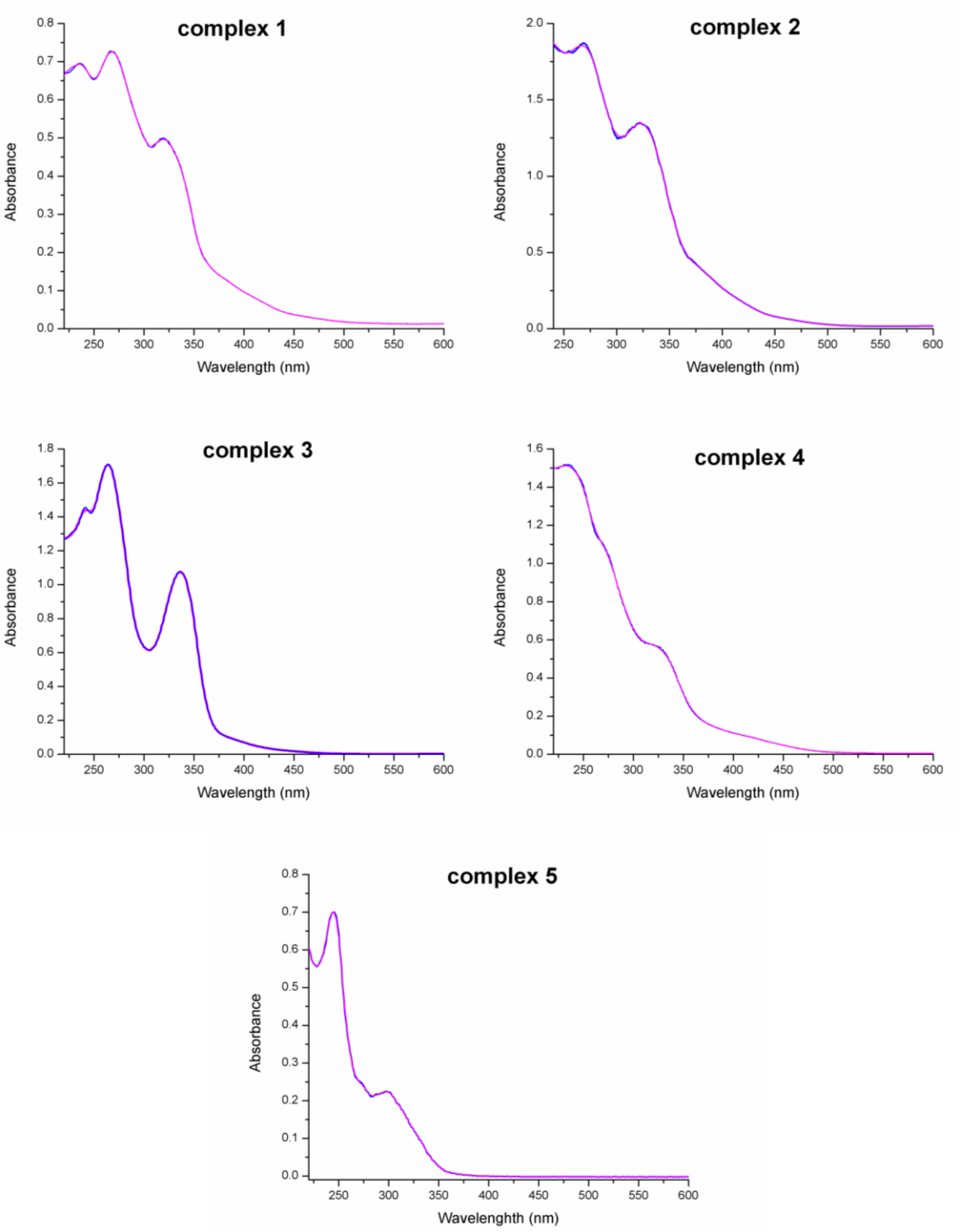

Figure S10. The UV-Vis spectroscopy data for complexes **1**–**5** in DMSO/H_2O 0.5 : 100 (*v*/*v*) at 298 K. First measurement (blue), after 24 h (pink).

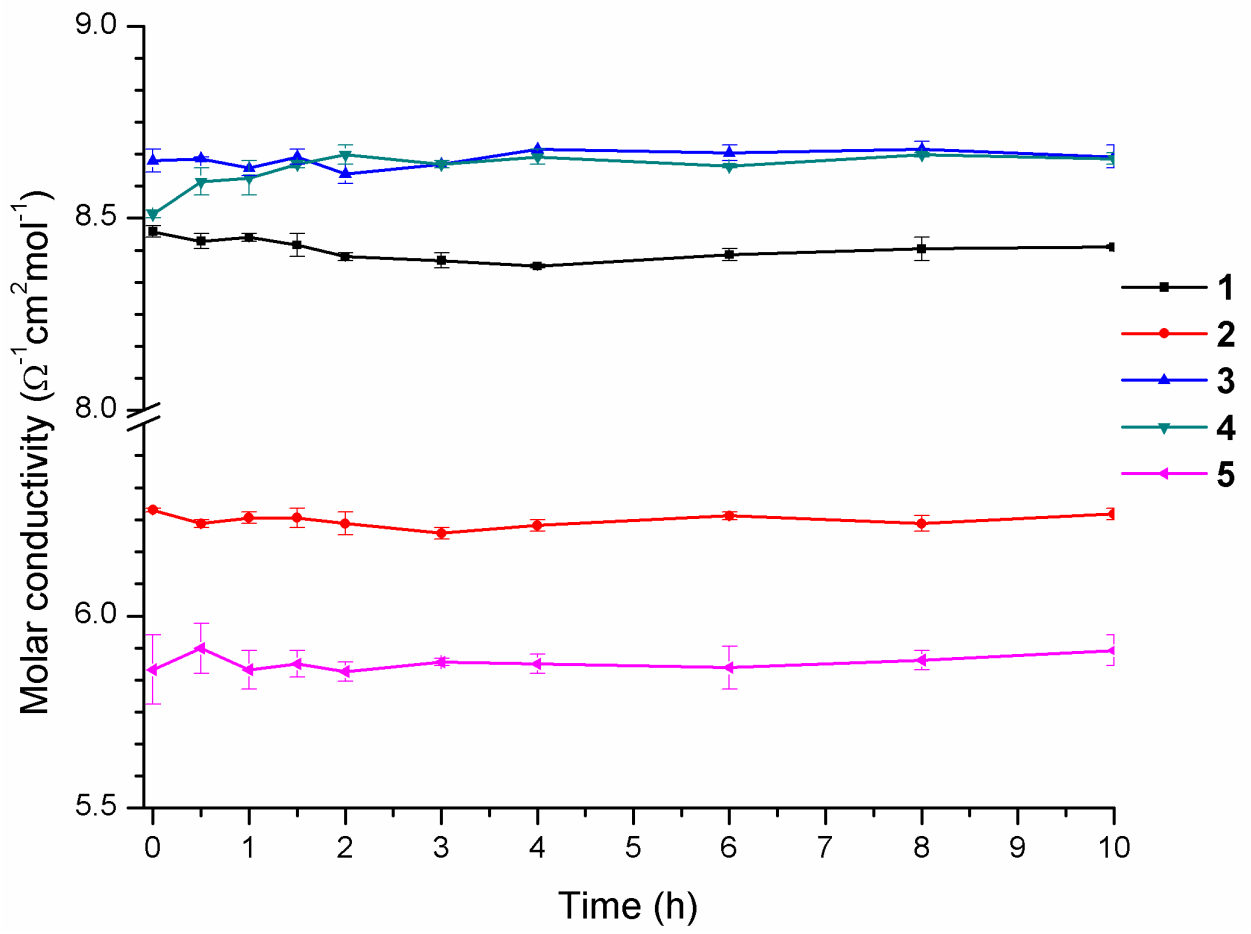

Figure S11. The molar conductivity plot for complexes **1**–**5** vs. time.

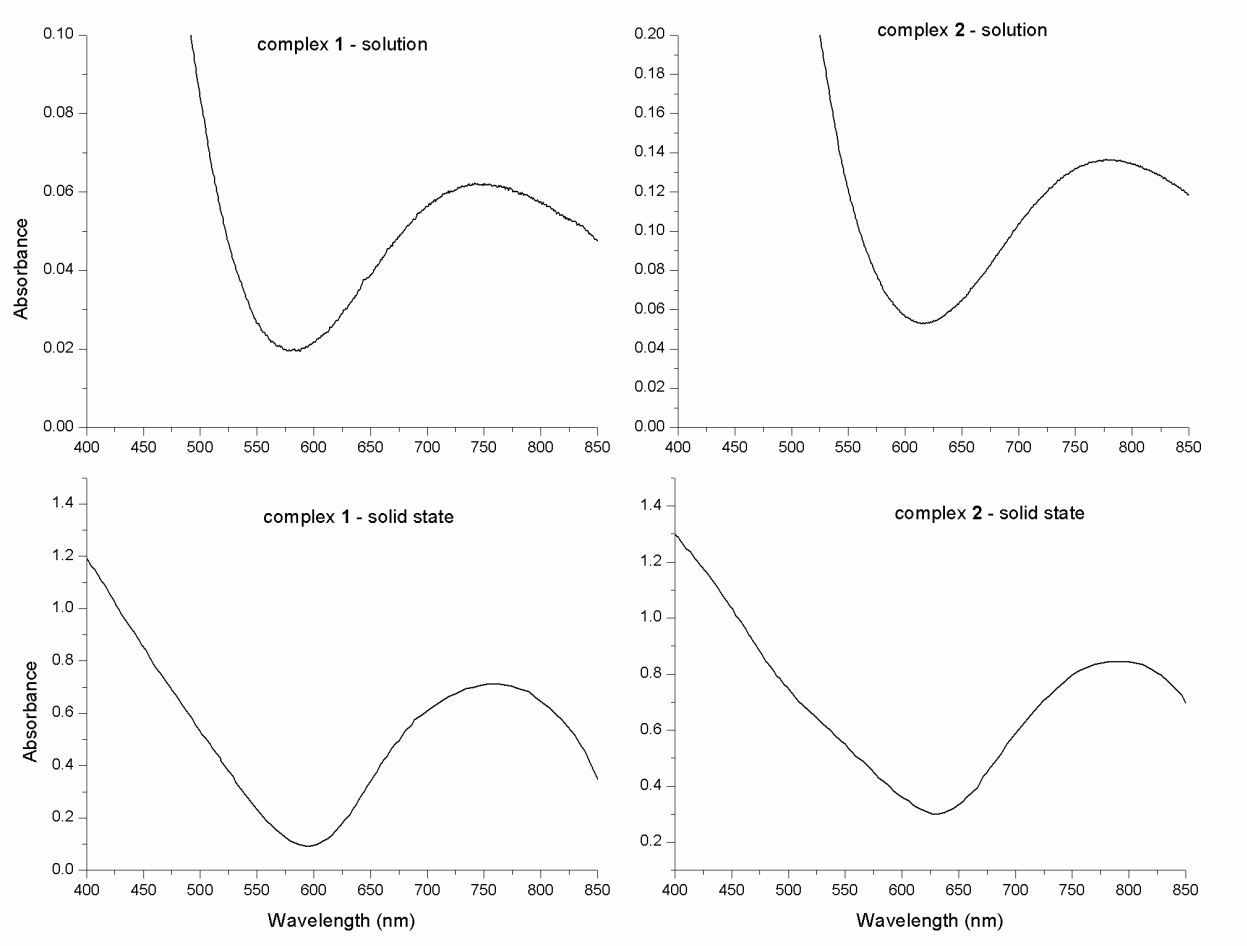

Figure S12. The solid state diffuse reflectance spectra of complexes **1** and **2** (lower panels) and UV-Vis spectra of the same complexes in solution (upper panels).

Magnetic behavior

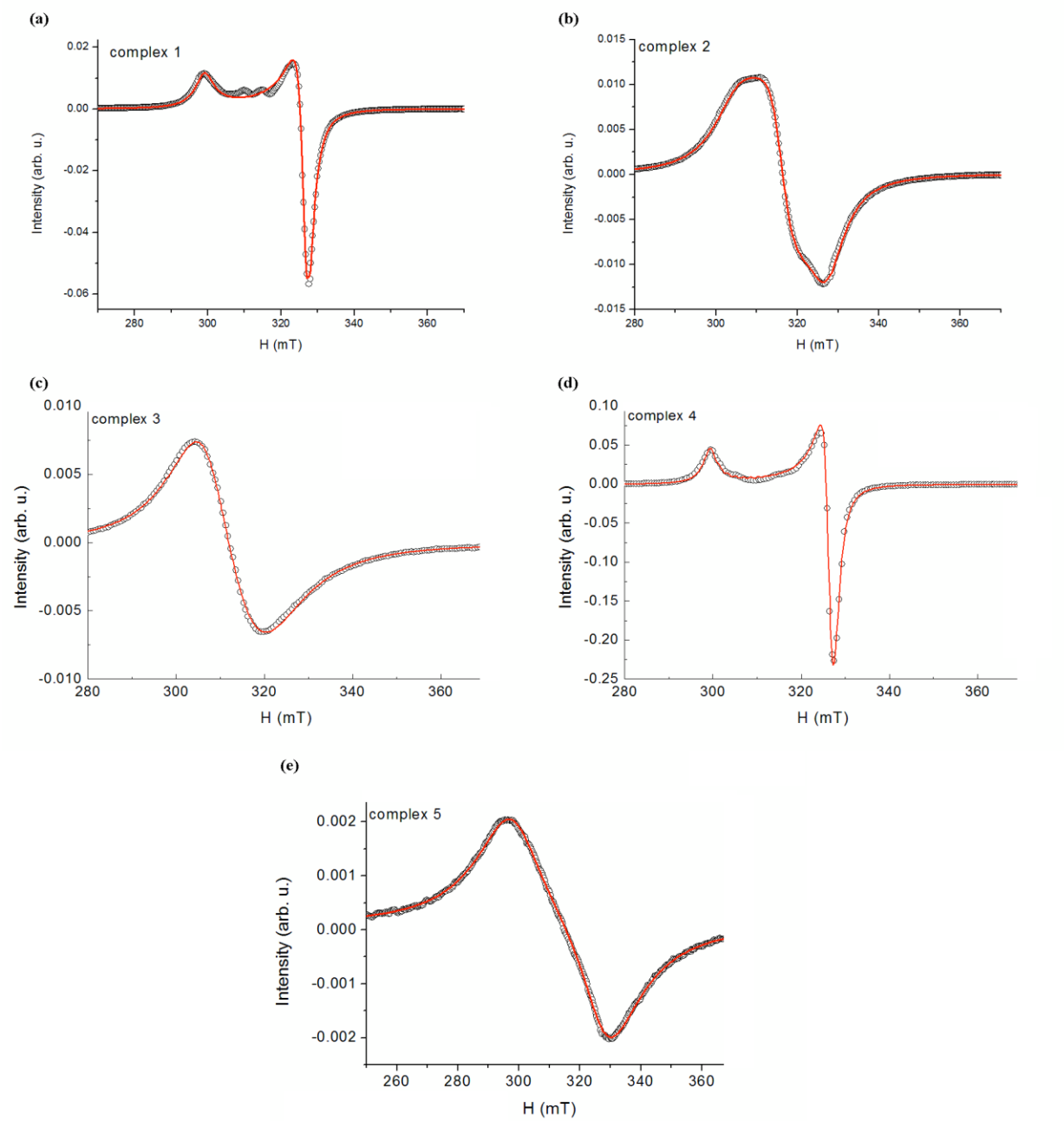

Figure S13. EPR spectra for complexes **1** (a), **2** (b), **3** (c), **4** (d) and **5** (e) with corresponding simulations plotted as red solid lines.

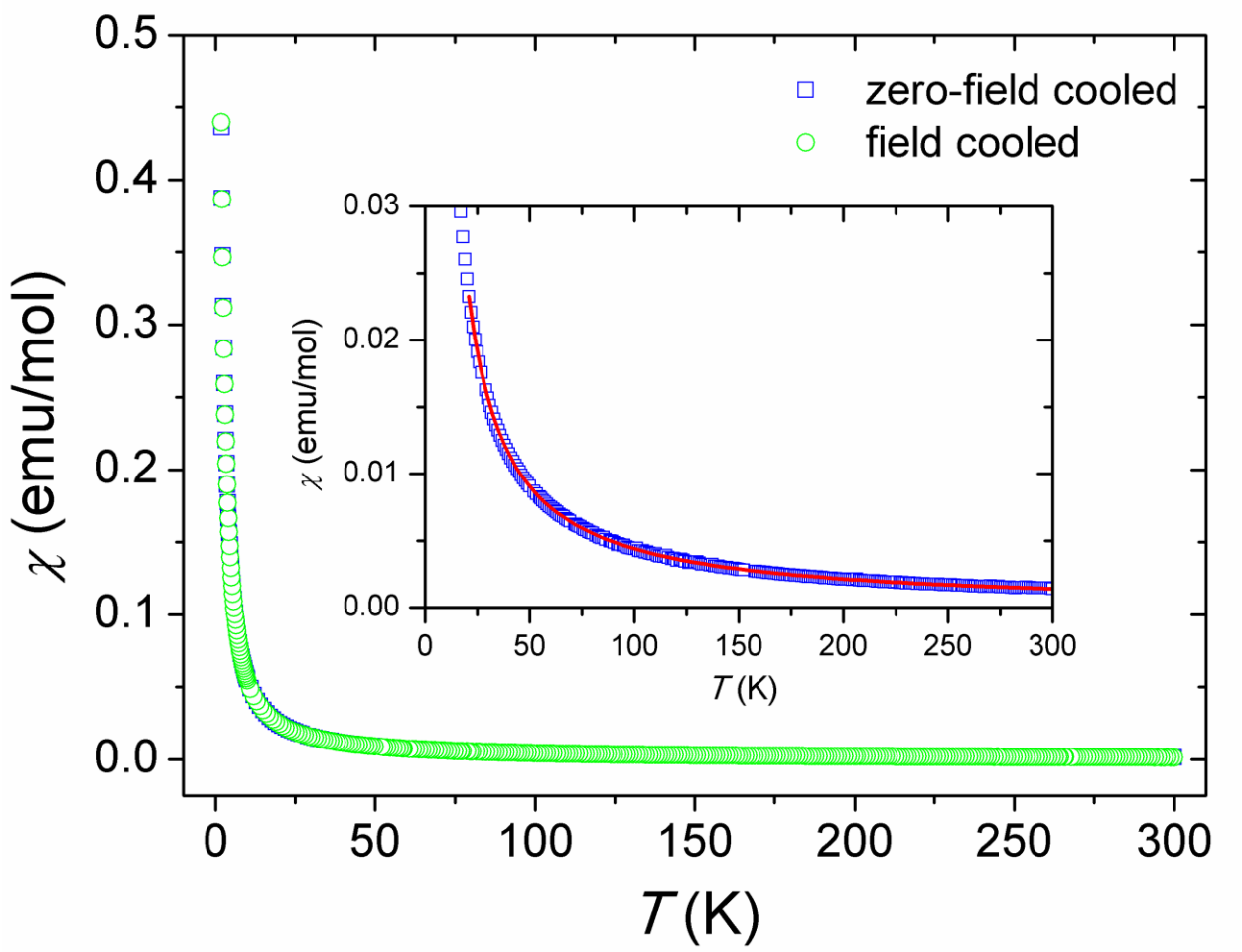

Figure S14. Temperature dependence of zero-field cooled (open blue squares) and field cooled susceptibility (open green circles) for complex **3**. A fit of the zero-field cooled curve with the Curie-Weiss law above 20 K is shown as a red full line in the inset.

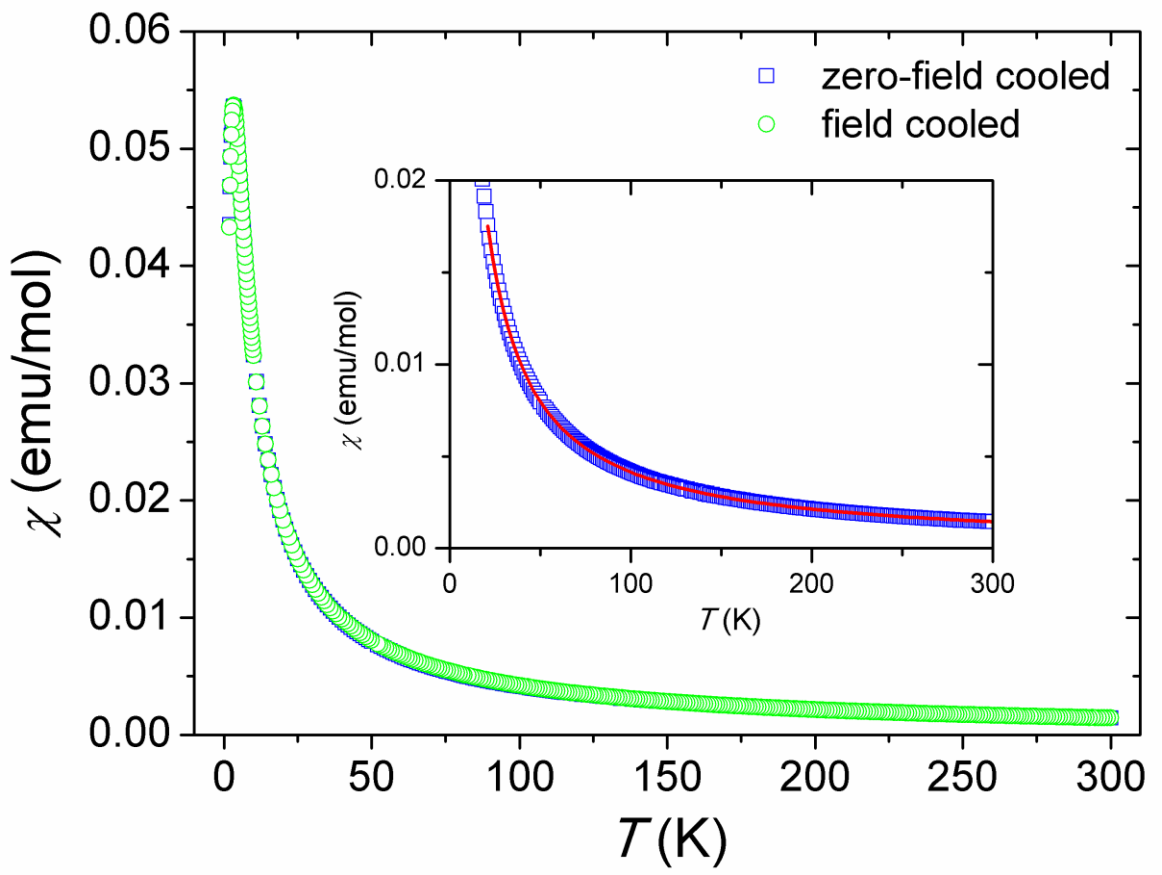

Figure S15. Temperature dependence of zero-field cooled (open blue squares) and field cooled susceptibility (open green circles) for complex **4**. A fit of the zero-field cooled curve with the Curie-Weiss law above 20 K is shown as a red full line in the inset.

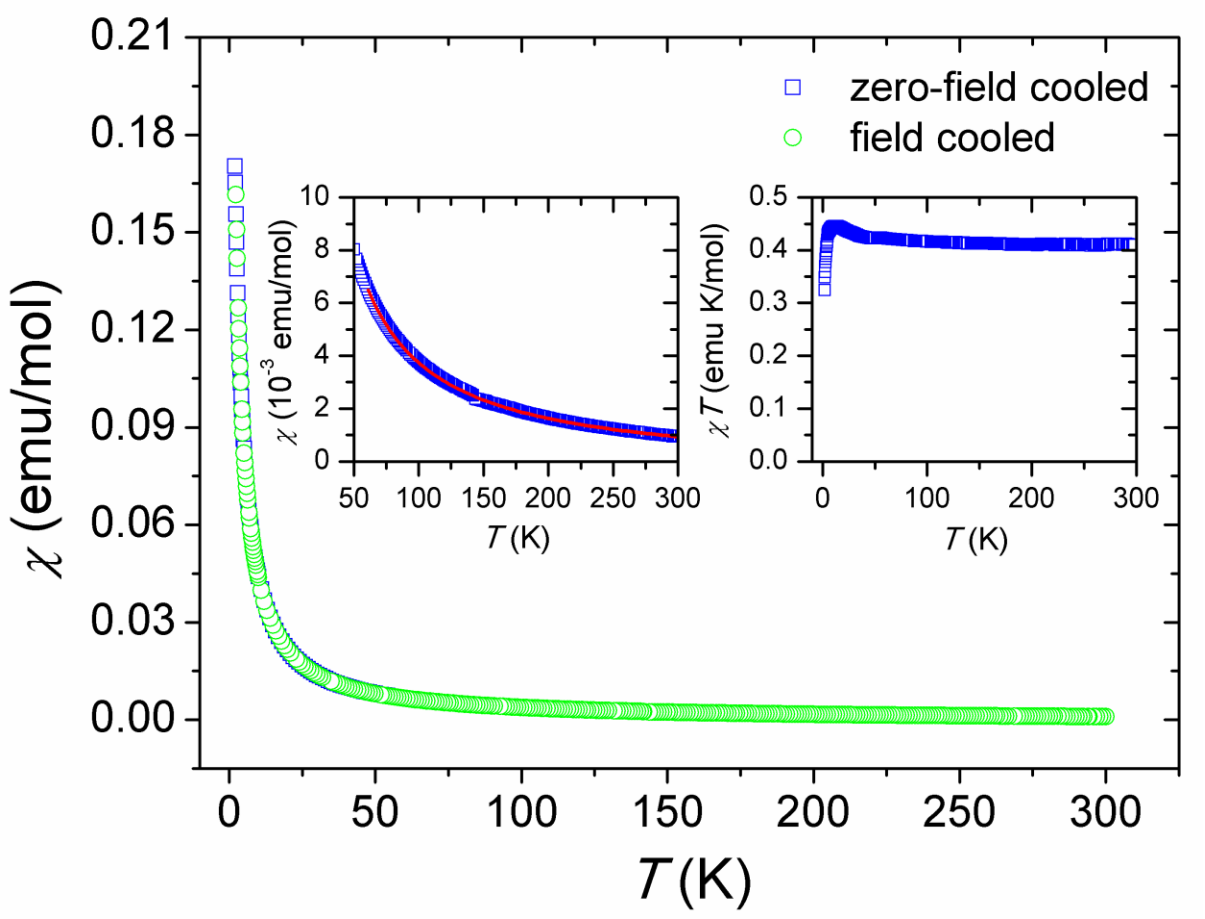

Figure S16. Temperature dependence of zero-field cooled (open blue squares) and field cooled susceptibility (open green circles) for complex **5**. A fit of the zero-field cooled curve with the Curie-Weiss law above 60 K is shown as a red full line in the left inset. The $\chi T(T)$ plot is shown in the right inset.

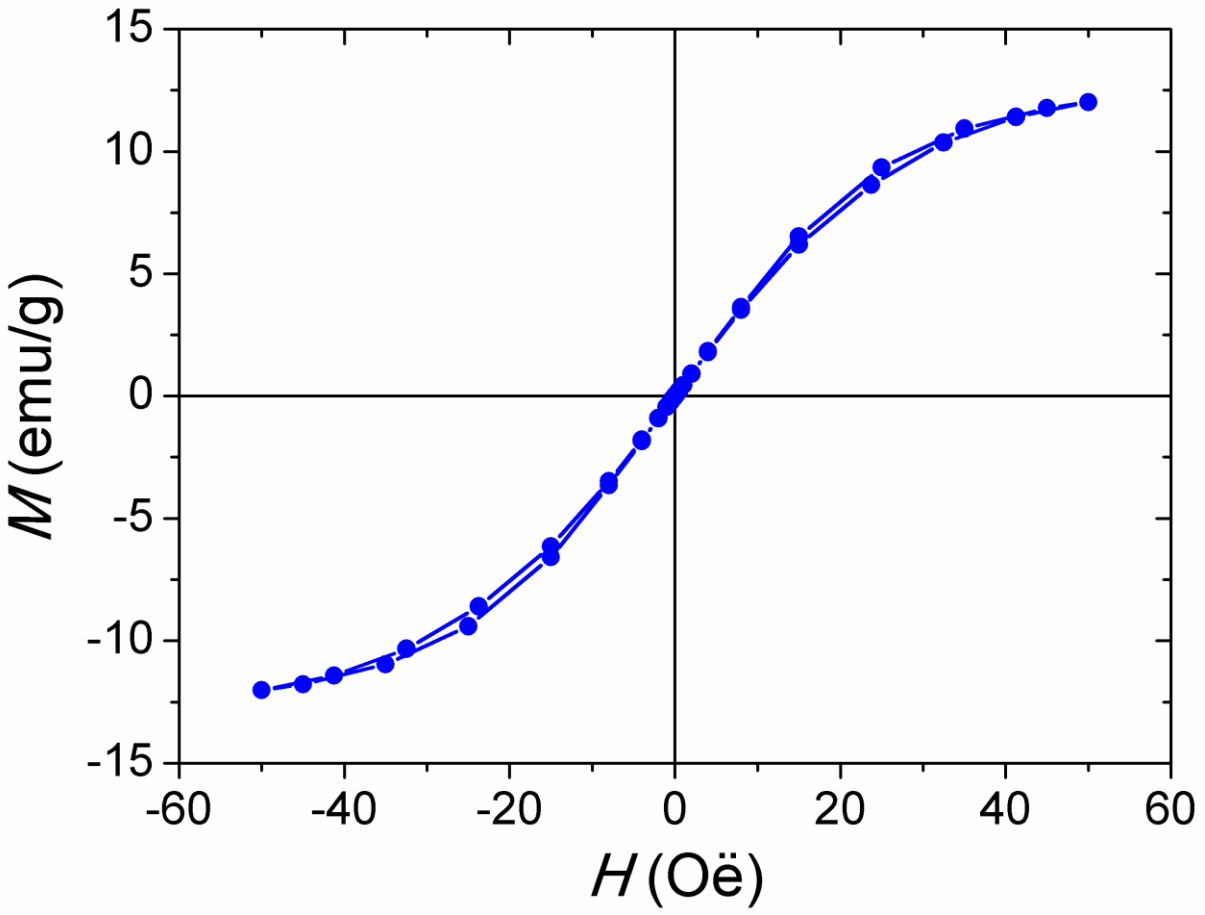

Figure S17. Magnetization curve for complex **5** measured at 2 K.

DFT calculations

Table S4. Summary of the DFT optimization results for the complexes **1**–**5**

Bond	Distance (Å)	*N*[a]	Angles (°)
$[CuCl_2(aphaOMe)]$ (**1**)			
Cu–Cl	2.18 (2.24)[b]	2 / 1	θ (Cl–Cu–Cl): 94.6 (95.4)
Cu–N	2.00 (2.01)	2 / 2	θ (Cl–Cu–N): 93.1 (95.1)
		1	θ (N–Cu–N): 79.9 (79.3)
$[Cu_2Cl_4(aphaOMe)_2]$ (**2**)			
Cu···Cu	3.56 (3.64)	1 / 2	θ (Cu–Cl–Cu): 88.5 (94.4)
Cu–Cl	2.46 (2.39)	6 / 4	θ (Cl–Cu–N): 95.1 (94.6)
Cu–N	2.13 (2.03)	4 / 2	θ (N–Cu–N): 76.9 (79.3)
$[CuCl_2(fphaOEt)]$ (**3**)			
Cu–Cl	2.26 (2.24)	2 / 1	θ (Cl–Cu–Cl): 97.8 (93.9)
Cu–N	2.12 (2.04)	2 / 2	θ (Cl–Cu–N): 94.9 (91.9)
		1	θ(N–Cu–N):77.3 (79.8.6)
$[CuCl_2(aphaOEt)]$ (**4**)			
Cu–Cl	2.26 (2.24)	2 / 1	θ (Cl–Cu–Cl): 97.4 (95.0)
Cu–N	2.11 (2.031)	2 / 2	θ (Cl–Cu–N): 94.6 (93.4)
		1	θ (N–Cu–N): 76.9 (79.3)
$[Cu_2Cl_4(qahaOEt)_2]$ (**5**)			
Cu···Cu	3.55 (3.44)	1 / 2	θ (Cu–Cl–Cu): 93.4 (92.8)
Cu–Cl	2.34 (2.34)	6 / 4	θ (Cl–Cu–N): 90.1 (89.5)
Cu–N	2.17 (2.06)	4 / 2	θ (N–Cu–N): 80.9 (80.3)

[a] *N* = number of bonds / angles. [b] Values obtained from X-ray diffraction analysis are given in parenthesis.